ACS APPLIED MATERIALS & INTERFACES

Research Article

www.acsami.org

Directly-Grown and Square-Patterned Arrays of Metal Oxide Nanowires for High-Performance Catalyst Support Platforms

Sang Ho Lee,[†] Eun Ja Lim,[†] Yong-Ryun Jo, Bong-Joong Kim, and Won Bae Kim*

School of Materials Science and Engineering and Research Institute for Solar and Sustainable Energies, Gwangju Institute of Science and Technology (GIST), Gwangju 500-712, Republic of Korea

Supporting Information

ABSTRACT: This research reports novel and efficient electrocatalyst support systems. Tin dioxide nanowires grown directly on current collecting substances are introduced as high-performance support platforms. For this propose, palladium or platinum catalysts are impregnated on these nanowire scaffolds and exhibit improved electrocatalytic performance for methanol oxidation in alkaline and acidic environments. These nanowire support platforms could be demonstrated to maximize the electrocatalytic activity because of the effective charge transport provided by the direct connection between the nanowire supports and current collectors. More significantly, grid-patterned nanowire arrays grown directly on current collectors are, for the first time, demonstrated as a milestone to enhance the electrocatalytic performance. The empty space between the patterned nanowire arrays acts as a channel to facilitate the electrolyte diffusion. The metal catalysts incorporated into the patterned nanowire supports show an 8-fold improvement in the catalytic performance for methanol electrooxidation, most likely because of the synergetic effects of the enhanced charge transport and mass transfer attributed to the structural advantages of the patterned nanowire array supports.

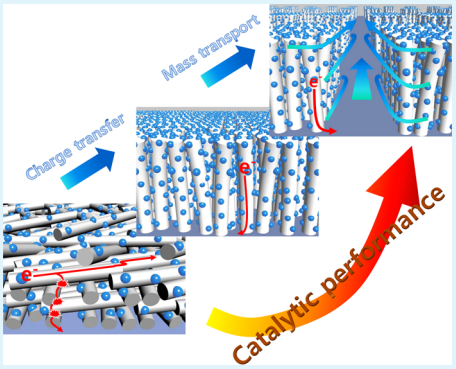

KEYWORDS: *directly grown and patterned SnO_2 nanowire supports, Pd or Pt catalysts, methanol oxidation, improved charge transport, enhanced mass transfer*

1. INTRODUCTION

Recently, metal oxides have attracted considerable scientific interest as electrocatalyst support materials in the fields of direct alcohol oxidation, taking their advantages of low cost, good electrical conductivity, and excellent stability in both alkaline and acidic media.[1−6] Moreover, metal oxide supports can provide oxygenated species in the catalytic system, which allows for the efficient oxidation of intermediate species adsorbed on the metal catalysts.[7,8] A wide range of metal oxide structures such as nanoparticles, nanowires, and nanotubes have been utilized for valuable electrocatalyst supports.[9−13] Unfortunately, however, these support structures have been randomly dispersed and densely loaded on working electrodes. This stack of the catalytic supports can cause high electrical contact resistance at the interfaces of the adjacent structures and can induce large mass transfer resistance for liquid reactants, which leads to a decline in the electrocatalytic performance.

One-dimensional (1D) nanostructure arrays formed directly on current collecting substances are of enormous interest in nanoscience and nanotechnology due to their large specific active surfaces combined with the enhanced charge transport resulting from the strong electronic connection between the conducting bodies and current collectors. To take advantage of the high surface areas and improved electronic conductivity, these 1D nanoscale platforms have been widely employed as advanced building blocks for energy storage devices,[14−19] chemical sensors,[20−23] and photoelectronic applications.[24−29] In addition, efficient pathways made between these nanostructures could facilitate the diffusion of reactants, which can give rise to the synergetic effect on system performance.

In this work, highly efficient catalyst support platforms are developed by integrating metallic catalysts on conducting metal oxide nanowire (NW) scaffolds that are directly synthesized on current collecting substrates. Pd or Pt catalysts are impregnated on SnO_2 NW scaffolds, and the produced electrocatalytic systems are applied for methanol oxidation in alkaline and acidic media, respectively. Because of the enhanced charge transport behavior due to the direct connection of the conducting NWs and current collectors, these metal catalysts/metal oxide NW platforms exhibit improved electrocatalytic performances for methanol oxidation. Furthermore, patterned arrays of SnO_2 NW scaffolds are employed in the electrooxidation system as an advanced model of NW supports grown directly on current collectors. The metal catalysts impregnated on the patterned NW scaffolds exhibit outstanding performances in the electrocatalytic oxidation reactions. These improved performances could be ascribed to the enhanced

Received: June 5, 2014
Accepted: November 18, 2014
Published: November 18, 2014

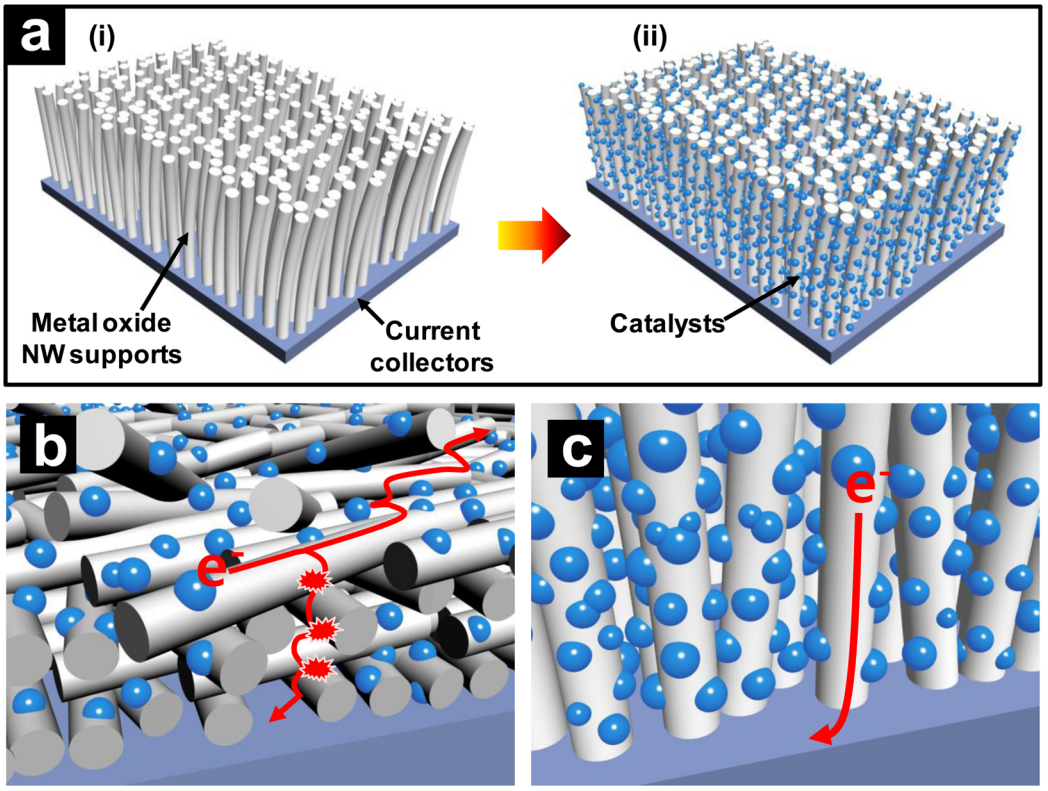

Figure 1. (a) Conceptual schemes for the proposed catalytic NW support platforms: (i) preparation of the metal oxide NWs grown directly on the current collecting substances and (ii) fabrication of the metal catalyst layers on the prepared NW supports. Illustrations of the (b) control samples and (c) proposed NW support platforms.

mass transfer of the liquid-phase reactants resulting from the flow channels formed between the patterned NW arrays. Notably, these directly grown and patterned arrays of metal oxide NW platforms could play a key role in improving material performances in diverse electrocatalytic reactions.

2. RESULTS AND DISCUSSION

Figure 1a shows schematic illustrations for the fabrication of the metal oxide NW support system proposed in this research, which involves deposition of metal catalysts on the metal oxide NW scaffolds that are rooting strongly on current collecting substrates. All the processes begin with the preparation of the metal oxide nanowire support platforms (Figure 1a(i)). Various metal oxide nanostructures have been formed on a wide range of substrates by chemical synthesis routes.[30−33] In this experiment, SnO_2 NWs were grown directly on stainless steel (SS) substrates by a thermal chemical vapor deposition (CVD). For demonstrating the proposed electrocatalytic support platforms, Pd or Pt catalyst layer was then deposited on the SnO_2 NW supports by a $NaBH_4$ reduction process (Figure 1a(ii)). Finally, these catalytic platforms on current collectors were directly applied as a working electrode for electrocatalytic reactions (refer to the schematic diagrams of the electrochemical system in Figure S1 of the Supporting Information). Graphical illustrations b and c in in Figure 1 depict two different support structures: (1) NWs randomly stacked over the SS current collectors (denoted as the "control"), which have been generally used in electrocatalytic systems (Figure 1b), and (2) NW scaffolds fabricated directly on the current collectors (denoted as the "SnO_2 NW/SS"), which is the new support design proposed here (Figure 1c). As shown in the conceptual illustration in Figure 1b, many contact resistances could exist between the adjacent interfaces of the support materials in the control samples, possibly leading to a decrease in the charge transport in the electrocatalytic system. Furthermore, the charge flow could be decentralized because of the random dispersion of the supports (see Figure 1b), which might not be able to effectively guide the electron stream up to current collectors. The stacks of NWs could also give rise to many hidden surfaces because of overlap between the supporting materials, which can result in a low utilization efficiency of the catalytic support platforms. In addition, a binding additive is required to fix the dispersed NW supports so that cohesion to the current collectors is maintained during the electrocatalytic reaction. On the other hand, the SnO_2 NW/SS (Figure 1c) could result in relatively lower contact resistance because of the strong contact between the NW support materials and current collectors, allowing for excellent electronic conductivity in the electrocatalytic system. Moreover, the strong connection between the NW supports and current collecting substrates could direct the electron flow along with their conducting backbones to the current collectors, resulting in fast charge transport. Because the SnO_2 NW/SS is fabricated directly on the current collectors, all the metal oxide surfaces are available for the catalysts and reactants. No binding additives are needed to anchor the NWs to the substrates. These advantages indicate that metal oxide NWs grown on current collectors can serve as a superior support platform for the active catalysts.

Figure 2 exhibits representative results for the Pd or Pt catalysts synthesized on the SnO_2 NW/SS supports. The typical scanning electron microscopy (SEM) images in Figures 2a-b show the Pd- and Pt-impregnated SnO_2 NW/SS, respectively. The original NW morphology appears to be intact even after

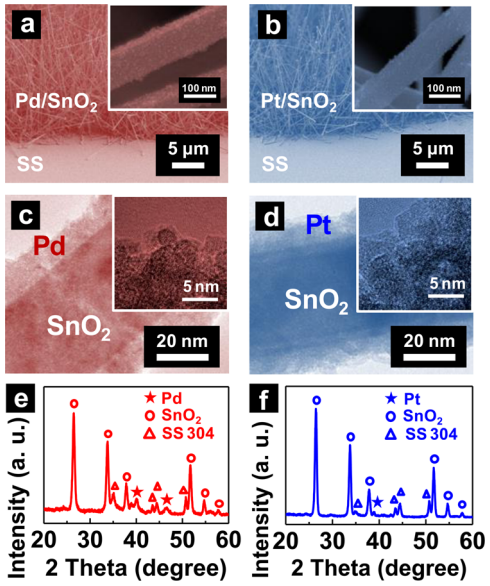

Figure 2. SEM images of (a) Pd and (b) Pt catalysts formed on the SnO_2 NW/SS scaffolds. The SnO_2 NW scaffolds have lengths of several tens of micrometers and diameters of approximately 50 to 200 nm. The inset images show magnified views of the catalysts on the scaffolds. TEM images of the (c) Pd and (d) Pt catalysts on the SnO_2 NWs. The insets show HRTEM images of the Pd and Pt catalysts (refer to Figures S4 and S5 in the Supporting Information). Representative XRD spectra of the (e) Pd and (f) Pt catalysts on the SnO_2 NW/SS.

the metal catalyst layers are fabricated on the NW scaffolds (see Figure S2 in the Supporting Information), revealing that the SnO_2 NWs are suitable supporting structures for the metal catalysts. The inset images in Figure 2a, b show the magnified views of the Pd and Pt catalysts fabricated on the NW surfaces, respectively. The metal oxide NW scaffold surfaces exhibit a textured topography after the metallic catalyst layers are deposited (see also Figure S2 in the Supporting Information), indicating that the metal catalysts are explicitly impregnated on the NW scaffolds. Detailed structures of the metal catalysts and NW supports were also observed by transmission electron microscopy (TEM). The TEM samples were prepared by detaching the Pd- or Pt-impregnated SnO_2 NWs from the SS current collectors and collecting them on TEM grids. First, the bare SnO_2 NWs fabricated on the SS substrates exhibit a smooth, straight surface morphology consisting of a single-crystalline phase, indicating that the NW scaffolds can provide an excellent conducting pathway for the electrons generated during the electrocatalytic reaction[34] (see TEM images in Figure S3 of the Supporting Information). Figure 2c, d show the TEM images of the Pd and Pt catalysts synthesized on the SnO_2 NW/SS, respectively. All the NW surfaces are covered with the metal catalyst layers, which were composed with metal nanoparticles of ca. 2−3 nm in diameter as seen in the insets of Figure 2c, d (also refer to Figures S4a and S5a in the Supporting Information). High-resolution TEM (HRTEM), selective area electron diffraction (SAED), and elemental mapping analysis further exhibit the detailed structure of these catalyst−supported NWs. In Figures S4a and S5a of the Supporting Information, HRTEM images show the distribution of tiny Pd and Pt nanoparticles, respectively, and the SAED patterns in the insets indicate that the Pd and Pt layers synthesized on the NW surfaces are comprised with metal nanoparticles of polycrystalline phases. As depicted in elemental mapping analysis of Figures S4b and S5b in the Supporting Information, the elements of Pd and Pt were evenly

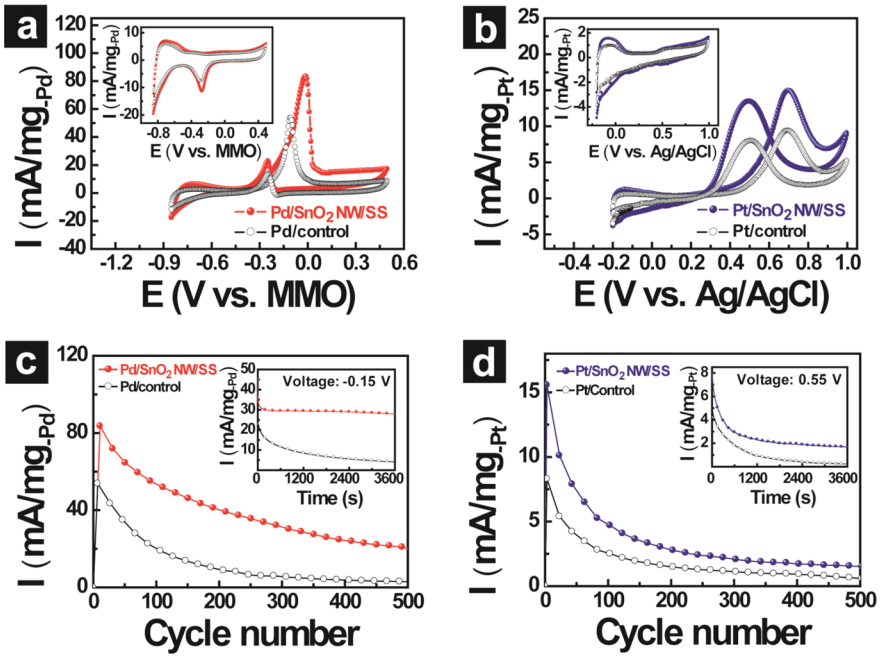

Figure 3. CV results for (a) Pd catalysts on the SnO_2 NW/SS and control in a mixture of 1.0 M CH_3OH and 1.0 M NaOH over a potential range of −0.85 to 0.5 V (vs Hg/HgO) at a scan rate of 50 mV/s and for (b) Pt catalysts on the SnO_2 NW/SS and control in a mixture of 2.0 M CH_3OH and 0.5 M H_2SO_4 over a range of −0.2 to 1.0 V (vs Ag/AgCl) at a scan rate of 50 mV/s. The insets show CV spectra in 1.0 M NaOH aqueous solution for the Pd and in 0.5 M H_2SO_4 aqueous solution for the Pt. Accelerated CV results for (c) Pd catalytic samples in a mixture of 1.0 M CH_3OH and 1.0 M NaOH and for (d) Pt catalytic samples in a mixture of 2.0 M CH_3OH and 0.5 M H_2SO_4. The insets show typical CA data for Pd samples at a constant potential of −0.15 V and for Pt samples at a controlled potential of 0.55 V.

dx.doi.org/10.1021/am5067089 | ACS Appl. Mater. Interfaces 2014, 6, 20634−20642

distributed over SnO_2 NW supports, respectively. Figure 2e, f present the X-ray diffraction (XRD) patterns of the Pd and Pt catalysts on the SnO_2 NW/SS, respectively. The XRD patterns for SnO_2, which are marked with empty circles, indicate that the NWs are in the tetragonal rutile phase (JCPDS Card No. 41−1445).[34] The XRD results in Figure 2e, f verifies that the Pd and Pt catalysts synthesized on the scaffolds are metallic phase (marked with star-shape). The diffraction peaks observed at approximately 2θ = 40 and 46° in Figure 2e correspond to the Pd (111) and Pd (200) lattices (JCPDS Card No. 87−0645), respectively,[35] and the peak detected at approximately 38° in Figure 2f corresponds to the main Pt (111) lattice (JCPDS Card No. 87−0644).[36] Only Pd and Pt catalyst, SnO_2 support, and SS substrate peaks are observed over the whole XRD scan range, implying that no impurity exists in the fabricated samples. On the basis of the SEM, TEM, and XRD results, it can be concluded that metallic Pd and Pt catalysts are explicitly fabricated on the SnO_2 NW/SS supports.

The Pd and Pt catalysts synthesized on the SnO_2 NW/SS were applied for electrooxidation of methanol in alkaline and acidic media, respectively (refer to the electrochemical system in Figure S1 of the Supporting Information), and the electrochemical performances of these catalyst systems were compared with those of the control samples under the same experimental conditions. Prior to the methanol oxidation reaction, the cyclic voltammetry (CV) measurements for the Pd and Pt catalysts on the SnO_2 NW/SS and control samples were performed in 1.0 M NaOH and 0.5 M H_2SO_4 aqueous solution, respectively. From these CV tests, the electrochemically active surface area (EASA) of the metal catalysts can be evaluated. The EASA value of the Pd catalysts was calculated by the Coulombic charge for the reduction of Pd−O monolayers,[37] which is based on the cathodic peaks between -0.1 and -0.4 V (the inset of Figure 3a), whereas the value of the Pt catalysts was estimated by the charge for the desorption of hydrogen monolayers,[38] which indicates the anodic peaks between -0.2 and 0.1 V (the inset of Figure 3b). Both the Pd and Pt catalysts formed on the SnO_2 NW/SS show higher EASA values than those on control samples, where the EASA values were normalized by the mass of Pd or Pt (see the detailed values in Table S1 and Table S2 of the Supporting Information). The improved EASA values might be attributed to the enhanced charge transport of SnO_2 NW/SS scaffolds due to the strong connection of these NWs to the SS current collector. The electrocatalytic activities of the Pd catalysts synthesized on the SnO_2 NW/SS and the control sample were investigated by CV measurements in a solution mixture of 1.0 M CH_3OH and 1.0 M NaOH. In the CV curves for the Pd-catalyzed methanol oxidation reaction (Figure 3a), two peaks that follow the typical oxidation trends of Pd catalysts in an alkaline environment are observed. The highest current density in the forward direction corresponds to methanol oxidation, while the current density in the backward direction is attributed to the oxidation of carbonaceous residues on the catalyst surface.[39,40] In the CV results, the Pd catalysts on the SnO_2 NW/SS have lower onset potentials than the control sample (refer to the detailed values in Table S1 of the Supporting Information), indicating that the Pd catalysts on the SnO_2 NW/SS can oxidize methanol more easily than the control sample. Also, this catalyst system exhibits a much higher Pd-mass-normalized activity for methanol oxidation than the control sample (see Table S1 in the Supporting Information), which could be attributed to the improved charge transport behavior of the proposed catalyst system. Furthermore, the intrinsic electrocatalytic activity of the metal catalysts on the SnO_2 NW/SS, which was obtained by normalizing their EASA values, is also higher than that of the control (see Table S1 and Figure S9 in the Supporting Information). Similar trends are also observed for the Pt catalysts based on CV investigations in 2.0 M CH_3OH and 0.5 M H_2SO_4 solution mixture as shown in Figure 3b, which presents the typical forward and backward sweeping curves for methanol oxidation by Pt catalysts under acidic conditions.[41,42] It is clearly shown that the Pt on the SnO_2 NW/SS exhibits a remarkably improved electrooxidation performance in terms of the onset potentials and oxidation activity as compared with the control samples (see Table S2 in the Supporting Information). These electrocatalytic results indicate that the NW scaffolds grown directly on the current collecting substances are a promising support platform for improving the catalyst performance under both alkaline and acidic conditions. Figure 3c, d show the accelerated CV results for the Pd and Pt catalysts on the SnO_2 NW/SS and control samples, respectively, where the current profiles were plotted up to 500 cycles. Even after the repetitive cycling, the Pd or Pt catalysts on the SnO_2 NW/SS scaffolds maintained much higher electrocatalytic activity for the methanol oxidation than those on the control samples. Furthermore, chronoamperometry (CA) was carried out (the insets in Figures 3c, d), where constant electrode potentials of −0.15 and 0.55 V were applied for the Pd and Pt catalysts, respectively. The Pd or Pt catalysts on the SnO_2 NW/SS supports hold much higher current densities than those on the control samples. These results imply that the enhanced electrical properties of the NW supports grown directly on the current collectors could have a significant impact on maintaining the catalytic activity.

The charge transport behavior was analyzed using electrochemical impedance spectroscopy (EIS) measurements. In general, the size of semicircles in the high-medium frequency region of the Nyquist plots indicates the level of the charge transport resistance of the materials; specifically, a smaller circle represents lower contact and charge transport resistance.[43,44] Figure 4a presents the typical Nyquist curves of the Pd on the

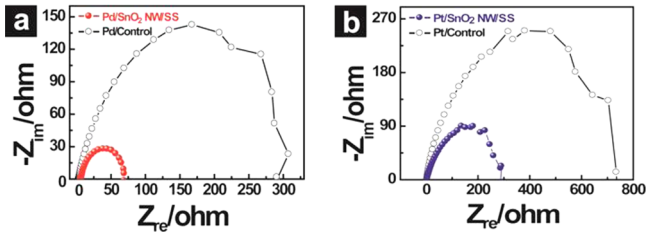

Figure 4. Nyquist plots of (a) Pd catalysts on the SnO_2 NW/SS and control support at a potential of −0.2 V (vs Hg/HgO) in a mixture of 1.0 M CH_3OH and 1.0 M NaOH and (b) Pt catalysts on the SnO_2 NW/SS and control support at a potential of 0.45 V (vs. Ag/AgCl) in a mixture of 2.0 M CH_3OH and 0.5 M H_2SO_4. The frequency was scanned from 10 kHz to 0.1 Hz with a constant amplitude of 10 mV.

SnO_2 NW/SS and the control sample, which were obtained at a potential of −0.2 V (vs Hg/HgO) in a mixture of 1.0 M CH_3OH and 1.0 M NaOH. Here, Z_{re} and Z_{im} represent the real and imaginary components of the impedance, respectively. The Pd on the SnO_2 NW/SS exhibits a very low charge transport resistance (Rct) of approximately 57.7 Ω cm^2, which is almost 4.5 times smaller than that of the control sample (approximately 260.8 Ω cm^2). This lower resistance demonstrates that

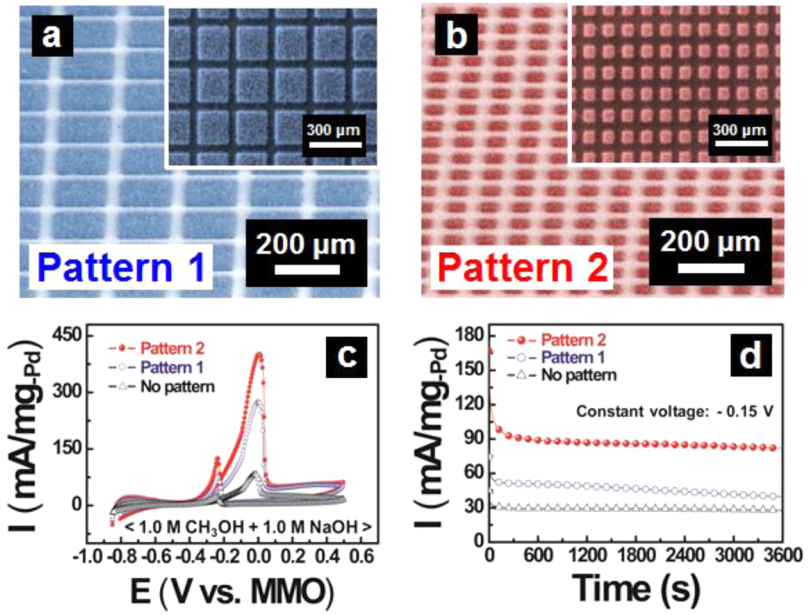

Figure 5. Tilted SEM images show the Pd-impregnated SnO_2 NW patterns with (a) grid areas of 150 × 150 μm^2 separated by channel width of 50 μm and (b) grid areas of 50 × 50 μm^2 separated by 50 μm. The insets are the magnified top view images of the grid-patterned NW support systems. (c) CV data for Pd catalysts on the patterned and nonpatterned scaffolds in a mixture of 1.0 M CH_3OH and 1.0 M NaOH over a potential range of −0.85 to 0.5 V (vs Hg/HgO) at a scan rate of 50 mV/s. (d) Representative CA results for Pd catalysts on the patterned and nonpatterned supports at a constant potential of −0.15 V.

the direct connection between the NW scaffolds and current collectors enhances the charge transport behavior. Additionally, the Pt catalysts exhibit an analogous trend in the charge transport resistance as shown in Figure 4b, which was measured at a potential of 0.45 V (vs Ag/AgCl) in a mixture of 2.0 M CH_3OH and 0.5 M H_2SO_4. The Pt catalysts on the SnO_2 NW/SS show a smaller semicircle than on the control sample with resistances (Rct) of approximately 319.7 and 719.1 Ω cm^2, respectively. These EIS results strongly support the fact that the enhanced charge transport behavior of the SnO_2 NW/SS system could contribute to the improved catalytic performance of the electrode reactions.

In this work, the SnO_2 NW supports were fabricated on metal seed layers, indicating that the positions of the NWs to be fabricated are determined by these seed layers.[45,46] The grid-patterned arrays of SnO_2 NW scaffolds were demonstrated by patterning the metal seed layers into the grid pattern, and they were used as further advanced support platform for electrocatalytic reactions. The patterned NW supports have scientific advantages in the fields of electrocatalysis. Importantly, the empty spaces formed between the grid-patterned NW arrays can serve as channels for the efficient mass transfer of chemical compounds, which could lead to the improvement in the electrocatalytic activity. Moreover, the pattern size and shape of the NW frameworks can be precisely modified by lithographical techniques, which allows to investigate the electrocatalytic performances with changing the support pattern geometries. Figures 5a-b present representative SEM images of patterned NW scaffolds with two different grid patterns on which the Pd catalysts were deposited. The fabrication procedure for the patterned NW arrays is depicted in Figure S11 in the Supporting Information. In Figure 5a, square-shaped patterns of approximately 150 × 150 μm^2 in area are uniformly arranged at a constant interval of approximately 50 μm (denoted as pattern 1). The grid patterns in Figure 5b are approximately 50 × 50 μm^2 in area and are separated by approximately 50 μm (denoted as pattern 2), which provide more paths across the grids when compared to pattern 1. Here, the height of these patterned SnO_2 NW supports is approximately 20 μm, which was estimated by the SEM measurement. The magnified images in the insets of panels a and b in Figure 5 explicitly show that pattern 2 has significantly more hollow channels than pattern 1. The effect of the patterned NW scaffolds is demonstrated by comparing the methanol oxidation performance with non-patterned NW scaffolds. Figure 5c exhibits the CV data for the Pd catalysts prepared on different scaffolds, including non-patterned NWs, pattern 1, and pattern 2. The Pd catalysts on the patterned scaffolds exhibit significantly higher Pd-mass-normalized oxidation activity than those on the nonpatterned NWs, indicating that the empty space in the patterned NW scaffolds could serve as excellent pathways for efficient electrolyte transfer. By fabricating more channels on the NW scaffolds (pattern 2), the current density in the oxidation reaction is improved, which might be attributed to the enhanced electrolyte mass transfer. Pattern 2 sample exhibits a 5-fold improvement in the oxidation activity compared to that of the nonpatterned scaffolds (see Table S3 in the Supporting Information). The mass of metal catalysts is decreased in the following order of no pattern > pattern 1 > pattern 2 because the total surface area of the SnO_2 NW supports for these metal catalysts is reduced by patterning the NW supports. This reduced mass loading of the catalysts might affect the mass-normalized catalytic activity, but this mass loading effect would be minor, from consideration of the intrinsic activity normalized by the EASA value for the no pattern, pattern 1, and pattern 2 (see Table S3 and Figure S13 in the Supporting Information). Surprisingly, the electrocatalytic activity of Pattern 2 is an 8-fold enhancement over that of the control sample (see Tables S1 and S3 in the Supporting Information). Similar trends are also observed for the Pt catalysts on

patterned NW supports for methanol oxidation in acidic conditions (see Figure S14 and Table S4 in the Supporting Information), implying that the patterned NW scaffolds are a quite versatile and promising metal oxide support system for improving the catalytic performance. Figure 5d shows the CA results for the Pd catalysts on the patterned and nonpatterned supports, where all the experiments were performed at a constant potential of −0.15 V (vs Hg/HgO). The current profiles of the Pd catalysts on the patterned supports have remained much higher than those of the catalysts on the nonpatterned scaffolds until the final stage, and extended hollow channels (pattern 2) increase the catalyst stability during the catalytic reaction (see Figure S15 in the Supporting Information).

Figure 6 shows a correlation between the electrocatalytic activity and the flow channel. Here, the channel area fraction

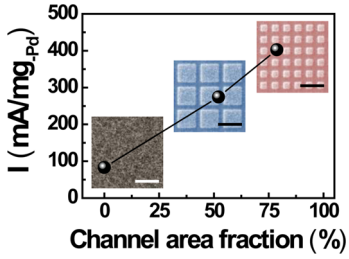

Figure 6. Relation between the electrocatalytic activity and the flow channel in the Pd/SnO_2 NW electrode systems. SEM images exhibit differently patterned Pd/SnO_2 NW electrodes (i.e., no pattern, pattern 1, and pattern 2). Here, the apparent areas of the flow channels were evaluated from these SEM images. All of the scale bars indicate 200 μm.

indicates the ratio of the flow channel areas to the total areas, where the flow channel areas were calculated by subtracting the pattern areas of Pd/SnO_2 NW arrays from the entire electrode areas. The electrocatalytic activity represents the forward peak current density for methanol oxidation of these Pd/SnO_2 NW electrodes. As the flow channels are increased in the catalytic NW electrode systems, the electrocatalytic activities are also accordingly increased. This result clearly demonstrates that the enhanced electrolyte mass transfer through the flow channels should contribute to the improvement in the electrooxidation activity.

Graphical illustrations in Figure 7a, b depict simplified electrode structures with nonpatterned and grid-patterned Pd/SnO_2 NW supports, respectively. The electrolyte can easily and efficiently diffuse through the hollow channels between the patterned NW electrodes (Figure 7b), which could improve the mass transfer of the electrolyte. The effect of the patterned NW supports on the electrolyte mass transfer was quantitatively estimated by modified CV measurements,[47−53] which was used in other reports for the Pd catalysts on pattern 2, pattern 1, and nonpatterned NW supports. Figure 7c shows the correlation between the normalized charges and scan rates for the methanol oxidation. Here, Q_x indicates the integrated charge of the forward peak at different scan rates (e.g., 5, 10, 15, 20, 50, 100, and 200 mV/s), and Q_{max} represents the maximum charge of the forward peak at the scan rate of 5 mV/s. This relation (Q_x/Q_{max}) clearly shows how effectively the liquid-phase electrolyte penetrates into and spreads out over catalyst−supported electrode structures.[47−53] Before the electrochemical tests, the samples were immersed in the electrolyte for a few

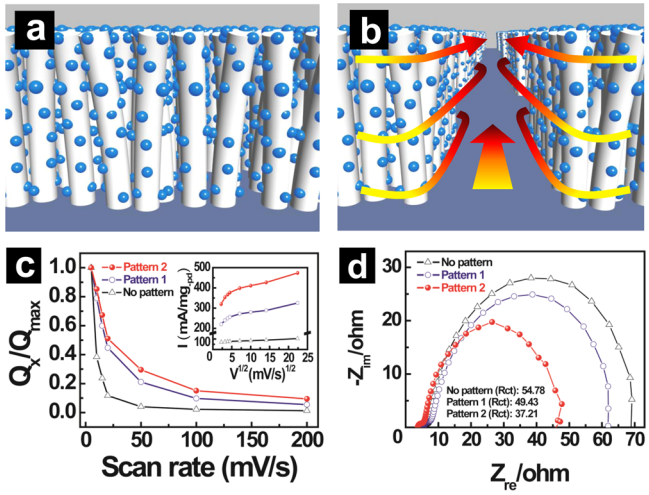

Figure 7. Schematic illustrations of (a) nonpatterned electrodes and (b) patterned ones with possible electrolyte flow path. (c) Normalized charge plots of the forward current against the scan rate for methanol oxidation of Pd catalysts on the differently patterned NW supports. The inset shows the correlation between the forward peak current density and the square root of the scan rate. (d) Representative Nyquist plots of Pd catalysts on the patterned and nonpatterned supports. The frequency range was 10 kHz to 0.1 Hz, and the amplitude was fixed at 10 mV.

minutes in order to release the inner pressure or any trapped air. In Figure 7c, the charge ratio (Q_x/Q_{max}) for the Pd/nonpatterned NWs is more rapidly declined with increasing scan rates than those for the Pd/patterned arrays. These results indicate that the electrooxidation of methanol for nonpatterned NW supports is more limited by mass transfer, whereas the patterned NW arrays allow for facile diffusion of the methanol molecules. The validity of the enhanced mass transfer of the patterned NW scaffolds can be further examined by plotting the forward peak current density against the square root of the scan rate.[48,51,53] In the inset of Figure 7c, the current density for the nonpatterned NW electrodes is rather linear with the square root of the scan rate. This implies that the electrocatalytic performance is controlled by the reactant concentration. On the other hand, the correlations for the patterned NW electrodes display parabolic curves at the low scan rate range, revealing that this electrooxidation activity is limited by the activation polarization of the electrocatalyst itself rather than by the mass transfer. Importantly, the relationship for pattern 2 draws a more curved behavior in the range of low scan rates due to more enhanced mass transfer of the liquid reactants. The patterned NW electrodes can also provide larger contact sites for the electrocatalytic reactants, which could lead to a decrease in the contact resistance for the electrolytes. The improved contact resistance was examined by EIS measurements on the different patterning features, and the results are shown in Figure 7d. The charge transport resistance of pattern 2 is approximately 37.2 Ω cm^2, which is smaller by almost 33 and 55% than those of pattern 1 (49.4 Ω cm^2) and nonpatterned NW scaffolds (57.8 Ω cm^2), respectively.

3. CONCLUSION

In summary, new and efficient metal oxide NW support systems were developed by growing SnO_2 NWs directly on current collecting substances. The Pd or Pt catalysts fabricated on these NW scaffolds exhibited the enhanced catalytic activity

for methanol oxidation in alkaline and acidic conditions, respectively, indicating that this NW scaffold system could improve the catalytic performance due to the enhanced electronic conductivity provided by the direct connection between the NW supports and current collectors. Importantly, the grid-patterned NW arrays were introduced as an advanced model for the metal oxide scaffolds formed directly on current collectors. The metal catalysts impregnated on these patterned supports exhibited an 8-fold increase in the oxidation activity, which might be attributed to the improved mass transfer of liquid reactants through the hollow channels formed between the patterned NW arrays, indicating that our new catalyst support system of directly grown and patterned metal oxide nanoarchitecture arrays could play an important role in enhancing the electrocatalytic performance in a wide range of electrochemical applications.

4. EXPERIMENTAL SECTION

Preparation of the SnO_2 NW Scaffolds. The SnO_2 NWs were fabricated by the thermal CVD process.[34] First, thin Au seed layers (approximately 5 nm) were deposited on a SS substrate by an electron-beam evaporator. The Au-deposited SS substrate was laid on a 2:1 powder mixture (by weight) of SnO_2 and graphite that was loaded on an alumina boat. The alumina boat was then loaded at the center of a horizontal quartz tube. Here, the SS substrate was placed downstream (approximately 3−5 cm) from the center of the quartz tube. The furnace temperature was increased to 900 °C under a 100 sccm Ar gas flow (99.999% purity), and these conditions were maintained for 10−30 min. After the furnace was cooled to room temperature, light gray products were observed on the substrate. For preparing the control samples, SnO_2 NWs were first fabricated on a substrate. The as-grown SnO_2 NWs were then detached physically from the substrate and loaded by dispersing the SnO_2 NWs over a fresh SS substrate. The patterned NW arrays were grown on the prepatterned Au seed layers by thermal CVD under the same fabrication conditions. The detailed procedures for patterning the Au seed layers via photolithography are described in Figure S11 in the Supporting Information.

Fabrication of the Pd or Pt Catalyst over the SnO_2 NWs. The Pd or Pt catalysts were synthesized on the SnO_2 NW scaffolds by a $NaBH_4$ reduction method.[54−57] First, the Pd solution was prepared by dissolving $PdCl_2$ (0.0179 g) in 20 mL of a mixture of ultrapure water and 35 wt % HCl, and the Pt solution consisted of $H_2PtCl_6{\cdot}6H_2O$ (0.0196 g) dissolved in 20 mL of water. The metal ion precursor solutions were then dropped on the SnO_2 NW scaffold substrates. After evaporating the aqueous solvents in air, the precursors were converted into the metallic phases by reduction with 0.01 M $NaBH_4$ solution. For the electrochemical test in case of the control sample that contains randomly distributed NWs on the substrate, Nafion binding additives (ca. 0.005 mg) were used to enhance electronic contact of the NW supports during the catalytic reaction. The Nafion binder itself does not affect the electrooxidation activity of the control samples (see Figure S8 in the Supporting Information). The mass of the synthesized Pd or Pt was directly and precisely measured by using a microbalance (Sartorius microbalance M3P at a resolution of 0.005 mg), which was calculated by comparing the mass of the samples before and after the Pd or Pt deposition.

Characterization of the Methanol Oxidation Properties. The electrocatalytic performances of the synthesized metal catalysts on the proposed NW scaffold systems were evaluated using a Solartron Analytical instrument (AMETEK model 1470E) with a three-electrode cell system (refer to Figure S1 in the Supporting Information). The synthesized samples and a Pt wire were used as the working and counter electrodes, respectively. Reference electrodes of Hg/HgO (1.0 M KOH) and Ag/AgCl (3.0 M KCl) were employed for the Pd and Pt catalytic tests, respectively. Prior to the methanol oxidation reactions, all the Pd and Pt samples were activated in N_2-purged NaOH and H_2SO_4 solutions, respectively. For the Pd samples, the CV measurements were collected over a potential range from −0.85 to 0.5 V in a mixture of 1.0 M CH_3OH and 1.0 M NaOH, while the Pt CV measurements were performed over a range of −0.2 to 1.0 V in a mixture of 2.0 M CH_3OH and 0.5 M H_2SO_4. The CA measurements were performed under a constant potential of approximately −0.15 V for Pd and 0.55 V for Pt. The amplitude of the modulation potentials for the EIS measurements was fixed at 10 mV, and the frequency was changed from 10 kHz to 0.1 Hz.

■ ASSOCIATED CONTENT

Ⓢ Supporting Information

(1) Graphical illustration for the three-electrode cell system, (2) SEM images of the bare SnO_2 NWs, the Pd/SnO_2 NWs, and the Pt/SnO_2 NWs, (3) TEM image and SAED pattern of the SnO_2 NWs, (4) HRTEM, SAED, and elemental mapping analysis for the Pd/SnO_2 NWs and the Pt/SnO_2 NWs, (5) SEM images of the SnO_2 NW/SS and the control samples, (6) the effect of Au seeds on the electrocatalytic reactions, (7) the preparation of the control sample for electrochemical measurements, (8) summary of the Pd and Pt catalytic performance for Figures 3, (9) fabrication process of the patterned SnO_2 NW scaffolds, (10) CV results for the Pd formed on differently patterned supports in 1.0 M NaOH solution, (11) summary of the electrooxidation performance for the Pd on differently patterned support platforms in Figure 5, (12) the effect of the patterned NW scaffolds on the Pt catalysts, and (13) accelerated CV results for the Pd on the patterned NW scaffolds. This material is available free of charge via the Internet at http://pubs.acs.org.

■ AUTHOR INFORMATION

Corresponding Author

*E-mail: wbkim@gist.ac.kr.

Author Contributions

†S.H.L. and E.J.L. contributed equally.

Notes

The authors declare no competing financial interest.

■ ACKNOWLEDGMENTS

This work was supported by the National Research Foundation of Korea (NRF) grant funded by the Korea government (MSIP) (No. 2014R1A2A1A11052414) and by the Core Technology Development Program for Next-generation Solar Cells of Research Institute for Solar and Sustainable Energies (RISE), GIST.

■ REFERENCES

(1) Huang, H.; Liu, Y.; Gao, Q.; Ruan, W.; Lin, X.; Li, X. Rational Construction of Strongly Coupled Metal-Metal Oxide-Graphene Nanostructure with Excellent Electrocatalytic Activity and Durability. *ACS Appl. Mater. Interfaces* **2014**, *6*, 10258−10264.

(2) Lo, C.-P.; Ramani, V. SiO_2-RuO_2: A Stable Electrocatalyst Support. *ACS Appl. Mater. Interfaces* **2012**, *4*, 6109−6116.

(3) Sharma, S.; Pollet, B. G. Support Materials for PEMFC and DMFC Electrocatalysts. *J. Power Sources* **2012**, *208*, 96−119.

(4) Fan, Y.; Liu, J.; Lu, H.; Huang, P.; Xu, D. Hierarchical Structure SnO_2 Supported Pt Nanoparticles as Enhanced Electrocatalysts for Methanol Oxidation. *Electrochim. Acta* **2012**, *76*, 475−479.

(5) Jing, W.; Huang, W.; Xing, W.; Wang, Y.; Jin, W.; Fan, Y. Fabrication of Supported Mesoporous TiO_2 Membranes: Matching the Assembled and Interparticle Pores for an Improved Ultrafiltration Performance. *ACS Appl. Mater. Interfaces* **2009**, *1*, 1607−1612.

(6) Macak, J. M.; Barczuk, P. J.; Tsuchiya, H.; Nowakowska, M. Z.; Ghicov, A.; Chojak, M.; Bauer, S.; Virtanen, S.; Kulesza, P. J.; Schmuki,

P. Self-Organized Nanotubular TiO_2 Matrix as Support for Dispersed Pt/Ru Nanoparticles: Enhancement of the Electrocatalytic Oxidation of Methanol. *Electrochem. Commun.* **2005**, *7*, 1417−1422.
(7) Zhao, X.; Yin, M.; Ma, L.; Liang, L.; Liu, C.; Liao, J.; Lu, T.; Xing, W. Recent Advances in Catalysts for Direct Methanol Fuel Cells. *Energy Environ. Sci.* **2011**, *4*, 2736−2753.
(8) Shen, P. K.; Xu, C. Alcohol Oxidation on Nanocrystalline Oxide Pd/C Promoted Electrocatalysts. *Electrochem. Commun.* **2006**, *8*, 184−188.
(9) Sui, X.-L.; Wang, Z.-B.; Yang, M.; Huo, L.; Gu, D.-M.; Yin, G.-P. Investigation on C-TiO_2 Nanotubes Composite as Pt Catalyst Support for Methanol Electrooxidation. *J. Power Sources* **2014**, *255*, 43−51.
(10) Huang, S.-Y.; Ganesan, P.; Popov, B. N. Titania Supported Platinum Catalyst with High Electrocatalytic Activity and Stability for Polymer Electrolyte Membrane Fuel Cell. *Appl. Catal., B* **2011**, *102*, 71−77.
(11) Hung, W.-Z.; Chung, W.-H.; Tsai, D.-S.; Wilkinson, D. P.; Huang, Y.-S. CO Tolerance and Catalytic Activity of Pt/Sn/SnO_2 Nanowires Loaded on a Carbon Paper. *Electrochim. Acta* **2010**, *55*, 2116−2122.
(12) Saha, M. S.; Li, R.; Sun, X. Composite of Pt−Ru Supported SnO_2 Nanowires Grown on Carbon Paper for Electrocatalytic Oxidation of Methanol. *Electrochem. Commun.* **2007**, *9*, 2229−2234.
(13) Saha, M. S.; Li, R.; Cai, M.; Sun, X. High Electrocatalytic Activity of Platinum Nanoparticles on SnO_2 Nanowire-Based Electrodes. *Electrochem. Solid-State Lett.* **2007**, *10*, B130−B133.
(14) Kim, J. G.; Lee, S. H.; Kim, Y. M.; Kim, W. B. Fabrication of Free-Standing $ZnMn_2O_4$ Mesoscale Tubular Arrays for Lithium-Ion Anodes with Highly Reversible Lithium Storage Properties. *ACS Appl. Mater. Interfaces* **2013**, *5*, 11321−11328.
(15) Jiang, J.; Li, Y.; Liu, J.; Huang, X. Building One-Dimensional Oxide Nanostructure Arrays on Conductive Metal Substrates for Lithium-Ion Battery Anodes. *Nanoscale* **2011**, *3*, 45−58.
(16) Bonino, C. A.; Ji, L.; Lin, Z.; Toprakci, O.; Zhang, X.; Khan, S. A. Electrospun Carbon-Tin Oxide Composite Nanofibers for Use as Lithium Ion Battery Anodes. *ACS Appl. Mater. Interfaces* **2011**, *3*, 2534−2542.
(17) Meduri, P.; Pendyala, C.; Kumar, V.; Sumanasekera, G. U.; Sunkara, M. K. Hybrid Tin Oxide Nanowires as Stable and High Capacity Anodes for Li-Ion Batteries. *Nano Lett.* **2009**, *9*, 612−616.
(18) Chan, C. K.; Peng, H.; Liu, G.; Mcilwrath, K.; Zhang, X. F.; Huggins, R. A.; Cui, Y. High-Performance Lithium Battery Anodes Using Silicon Nanowires. *Nat. Nanotechnol.* **2008**, *3*, 31−35.
(19) Chan, C. K.; Zhang, X. F.; Cui, Y. High Capacity Li Ion Battery Anodes Using Ge Nanowires. *Nano Lett.* **2008**, *8*, 307−309.
(20) Wang, B.; Zhu, L. F.; Yang, Y. H.; Xu, N. S.; Yang, G. W. Fabrication of a SnO_2 Nanowire Gas Sensor and Sensor Performance for Hydrogen. *J. Phys. Chem. C* **2008**, *112*, 6643−6647.
(21) Choi, Y.-J.; Hwang, I.-S.; Park, J.-G.; Choi, K. J.; Park, J.-H.; Lee, J.-H. Novel Fabrication of an SnO_2 Nanowire Gas Sensor with High Sensitivity. *Nanotechnology* **2008**, *19*, 095508.
(22) Comini, E.; Sherveglieri, G. Metal Oxide Nanowires as Chemical Sensors. *Mater. Today* **2010**, *13*, 36−44.
(23) Comini, E. Integration of Metal Oxide Nanowires in Flexible Gas Sensing Devices. *Sensors* **2013**, *13*, 10659−10673.
(24) Kargar, A.; Sun, K.; Jing, Y.; Choi, C.; Jeong, H.; Zhou, Y.; Madsen, K.; Naughton, P.; Jin, S.; Jung, G. Y.; Wang, D. Tailoring n-ZnO/p-Si Branched Nanowire Heterostructures for Selective Photoelectrochemical Water Oxidation or Reduction. *Nano Lett.* **2013**, *13*, 3017−3022.
(25) Desai, U. V.; Xu, C.; Wu, J.; Gao, D. Hybrid TiO_2−SnO_2 Nanotube Arrays for Dye-Sensitized Solar Cells. *J. Phys. Chem. C* **2013**, *117*, 3232−3239.
(26) Wang, Y.-F.; Li, K.-N.; Wu, W.-Q.; Xu, Y.-F.; Chen, H.-Y.; Su, C.-Y.; Kuang, D.-B. Fabrication of a Double Layered Photoanode Consisting of SnO_2 Nanofibers and Nanoparticles for Efficient Dyesensitized Solar Cells. *RSC Adv.* **2013**, *3*, 13804−13810.
(27) Yu, P.; Chang, C.-H.; Su, M.-S.; Hsu, M.-H.; Wei, K.-H. Embedded Indium-Tin-Oxide Nanoelectrodes for Efficiency and Lifetime Enhancement of Polymer-Based Solar Cells. *Appl. Phys. Lett.* **2010**, *96*, 153307.
(28) Takanezawa, K.; Tajima, K.; Hashimoto, K. Efficiency Enhancement of Polymer Photovoltaic Devices Hybridized with ZnO Nanorod Arrays by the Introduction of a Vanadium Oxide Buffer Layer. *Appl. Phys. Lett.* **2008**, *93*, 063308.
(29) Law, M.; Greene, L. E.; Johnson, J. C.; Saykally, R.; Yang, P. Nanowire Dye-Sensitized Solar Cells. *Nat. Mater.* **2005**, *4*, 455−459.
(30) Kim, J. G.; Nam, S. H.; Lee, S. H.; Choi, S. M.; Kim, W. B. SnO_2 Nanorod-Planted Graphite: An Effective Nanostructure Configuration for Reversible Lithium Ion Storage. *ACS Appl. Mater. Interfaces* **2011**, *3*, 828−835.
(31) Jeong, S. M.; McDowell, M. T.; Cui, Y. Low-Temperature Self-Catalytic Growth of Tin Oxide Nanocones over Large Areas. *ACS Nano* **2011**, *5*, 5800−5807.
(32) Wang, Y.; Lee, J. Y.; Zeng, H. C. Polycrystalline SnO_2 Nanotubes Prepared via Infiltration Casting of Nanocrystallites and Their Electrochemical Application. *Chem. Mater.* **2005**, *17*, 3899−3903.
(33) Zhang, Y.; Wang, N.; Gao, S.; He, R.; Miao, S.; Liu, J.; Zhu, J.; Zhang, X. A Simple Method to Synthesize Nanowires. *Chem. Mater.* **2002**, *14*, 3564−3568.
(34) Lee, S. H.; Jo, G.; Park, W.; Lee, S. K.; Kim, Y.-S.; Cho, B. K.; Lee, T.; Kim, W. B. Diameter-Engineered SnO_2 Nanowires over Contact-Printed Gold Nanodots Using Size-Controlled Carbon Nanopost Array Stamps. *ACS Nano* **2010**, *4*, 1829−1836.
(35) Seo, M. H.; Choi, S. M.; Nam, S. H.; Kim, H. J.; Kim, W. B. Synthesis, Characterization, and Electrocatalytic Properties of a Polypyrrole-Composited Pd/C Catalyst. *Int. J. Hydrogen Energy* **2011**, *36*, 11545−11553.
(36) Lee, S. H.; Cho, B.; Yoon, S.; Jeong, H.; Jon, S.; Jung, G. Y.; Cho, B. K.; Kim, W. B. Printing of Sub-100-nm Metal Nanodot Arrays by Carbon Nanopost Stamps. *ACS Nano* **2011**, *7*, 5543−5551.
(37) Lim, E. J.; Kim, H. J.; Kim, W. B. Efficient Electrooxidation of Methanol and Ethanol Using MoO_x-Decorated Pd Catalysts in Alkaline Media. *Catal. Commun.* **2012**, *25*, 74−77.
(38) Lee, S. H.; Choi, S. M.; Yoon, S.; Jeong, H.; Jung, G. Y.; Cho, B. K.; Kim, W. B. Transfer Printing of Metal Nanoring and Nanodot Arrays for Use in Catalytic Reactions. *Chem. Commun.* **2014**, *50*, 8472−8475.
(39) Bianchini, C.; Shen, P. K. Palladium-Based Electrocatalysts for Alcohol Oxidation in Half Cells and in Direct Alcohol Fuel Cells. *Chem. Rev.* **2009**, *109*, 4183−4206.
(40) Zhu, C.; Guo, S.; Dong, S. PdM (M = Pt, Au) Bimetallic Alloy Nanowires with Enhanced Electrocatalytic Activity for Electro-Oxidation of Small Molecules. *Adv. Mater.* **2012**, *24*, 2326−2331.
(41) Herrero, E.; Franaszczuk, K.; Wieckowski, A. Electrochemistry of Methanol at Low Index Crystal Planes of Platinum: An Integrated Voltammetric and Chronoamperometric Study. *J. Phys. Chem.* **1994**, *98*, 5074−5083.
(42) Tripković, A. V.; Popović, K. D.; Grgur, B. N.; Blizanac, B.; Ross, P. N.; Marković, N. M. Methanol Electrooxidation on Supported Pt and PtRu Catalysts in Acid and Alkaline Solutions. *Electrochim. Acta* **2002**, *47*, 3707−3714.
(43) Seland, F.; Tunold, R.; Harrington, D. A. Impedance Study of Methanol Oxidation on Platinum Electrodes. *Electrochim. Acta* **2006**, *51*, 3827−3840.
(44) Chen, A.; Russa, D. J. L.; Miller, B. Effect of the Iridium Oxide Thin Film on the Electrochemical Activity of Platinum Nanoparticles. *Langmuir* **2004**, *20*, 9695−9702.
(45) Huang, M. H.; Wu, Y.; Feick, H.; Tran, N.; Weber, E.; Yang, P. Catalytic Growth of Zinc Oxide Nanowires by Vapor Transport. *Adv. Mater.* **2001**, *13*, 113−116.
(46) Yang, P.; Yan, H.; Mao, S.; Russo, R.; Johnson, J.; Saykally, R.; Morris, N.; Pham, J.; He, R.; Choi, H.-J. Cotrolled Growth of ZnO Nanowires and Their Optical Properties. *Adv. Funct. Mater.* **2002**, *12*, 323−331.
(47) Bambagioni, V.; Bianchini, C.; Marchionni, A.; Filippi, J.; Vizza, F.; Teddy, J.; Serp, P.; Zhiani, M. Pd and Pt-Ru Anode Electrocatalysts

Supported on Multi-Walled Carbon Nanotubes and Their Use in Passive and Active Direct Alcohol Fuel Cells with an Anion-Exchange Membrane (Alcohol = Methanol, Ethanol, Glycerol). *J. Power Sources* **2009**, *190*, 241−251.
(48) Hu, F. P.; Wang, Z.; Li, Y.; Li, C.; Zhang, X.; Shen, P. K. Improved Performance of Pd Electrocatalyst Supported on Ultrahigh Surface Area Hollow Carbon Spheres for Direct Alcohol Fuel Cells. *J. Power Sources* **2008**, *177*, 61−66.
(49) Xu, M.-W.; Gao, G.-Y.; Zhou, W.-J.; Zhang, K.-F.; Li, H.-L. Novel Pd/β-MnO_2 Nanotubes Composites as Catalysts for Methanol Oxidation in Alkaline Solution. *J. Power Sources* **2008**, *175*, 217−220.
(50) Hu, F. P.; Cui, G.; Wei, Z.; Shen, P. K. Improved Kinetics of Ethanol Oxidation on Pd Catalysts Supported on Tungsten Carbides/Carbon Nanotubes. *Electrochem. Commun.* **2008**, *10*, 1303−1306.
(51) Hu, F.; Ding, F.; Song, S.; Shen, P. K. Pd Electrocatalyst Supported on Carbonized TiO_2 Nanotube for Ethanol Oxidation. *J. Power Sources* **2006**, *163*, 415−419.
(52) Zhang, K.-F.; Guo, D.-J.; Liu, X.; Li, J.; Li, H.-L.; Su, Z.-X. Vanadium Oxide Nanotubes as the Support of Pd Catalysts for Methanol Oxidation in Alkaline Solution. *J. Power Sources* **2006**, *162*, 1077−1081.
(53) Wang, Z.; Hu, F.; Shen, P. K. Carbonized Porous Anodic Alumina as Electrocatalyst Support for Alcohol Oxidation. *Electrochem. Commun.* **2006**, *8*, 1764−1768.
(54) Liu, H.; Koenigsmann, C.; Adzic, R. R.; Wong, S. S. Probing Ultrathin One-Dimensional Pd−Ni Nanostructures as Oxygen Reduction Reaction Catalysts. *ACS Catal.* **2014**, *4*, 2544−2555.
(55) Koenigsmann, C.; Semple, D. B.; Sutter, E.; Tobierre, S. E.; Wong, S. S. Ambient Synthesis of High-Quality Ruthenium Nanowires and the Morphology-Dependent Electrocatalytic Performance of Platinum-Decorated Ruthenium Nanowires and Nanoparticles in the Methanol Oxidation Reaction. *ACS Appl. Mater. Interfaces* **2013**, *5*, 5518−5530.
(56) Koenigsmann, C.; Santulli, A. C.; Sutter, E.; Wong, S. S. Ambient Surfactantless Synthesis, Growth Mechanism, and Size-Dependent Electrocatalytic Behavior of High-Quality, Single Crystalline Palladium Nanowires. *ACS Nano* **2011**, *5*, 7471−7487.
(57) Koenigsmann, C.; Santulli, A. C.; Gong, K.; Vukmirovic, M. B.; Zhou, W.-P.; Sutter, E.; Wong, S. S.; Adzic, R. R. Enhanced Electrocatalytic Performance of Processed, Ultrathin, Supported Pd-Pt Core−Shell Nanowire Catalysts for the Oxygen Reduction Reaction. *J. Am. Soc. Chem.* **2011**, *133*, 9783−9795.